doi:10.1093/brain/awz247 BRAIN 2019: 142; 2965–2978 | 2965

BRAIN
A JOURNAL OF NEUROLOGY

Agenesis of the putamen and globus pallidus caused by recessive mutations in the homeobox gene *GSX2*

Roberta De Mori,[1,*] Mariasavina Severino,[2,*] Maria Margherita Mancardi,[3] Danila Anello,[1] Silvia Tardivo,[1] Tommaso Biagini,[4] Valeria Capra,[5] Antonella Casella,[6] Cristina Cereda,[7] Brett R. Copeland,[8] Stella Gagliardi,[7] Alessandra Gamucci,[3] Monia Ginevrino,[1,6] Barbara Illi,[9] Elisa Lorefice,[10] Damir Musaev,[8] Valentina Stanley,[8] Alessia Micalizzi,[11] Joseph G. Gleeson,[8] Tommaso Mazza,[4] Andrea Rossi[2] and Enza Maria Valente[1,6]

*These authors contributed equally to this work.

Basal ganglia are subcortical grey nuclei that play essential roles in controlling voluntary movements, cognition and emotion. While basal ganglia dysfunction is observed in many neurodegenerative or metabolic disorders, congenital malformations are rare. In particular, dysplastic basal ganglia are part of the malformative spectrum of tubulinopathies and X-linked lissencephaly with abnormal genitalia, but neurodevelopmental syndromes characterized by basal ganglia agenesis are not known to date. We ascertained two unrelated children (both female) presenting with spastic tetraparesis, severe generalized dystonia and intellectual impairment, sharing a unique brain malformation characterized by agenesis of putamina and globi pallidi, dysgenesis of the caudate nuclei, olfactory bulbs hypoplasia, and anomaly of the diencephalic-mesencephalic junction with abnormal corticospinal tract course. Whole-exome sequencing identified two novel homozygous variants, c.26C>A; p.(S9*) and c.752A>G; p.(Q251R) in the *GSX2* gene, a member of the family of homeobox transcription factors, which are key regulators of embryonic development. *GSX2* is highly expressed in neural progenitors of the lateral and median ganglionic eminences, two protrusions of the ventral telencephalon from which the basal ganglia and olfactory tubercles originate, where it promotes neurogenesis while negatively regulating oligodendrogenesis. The truncating variant resulted in complete loss of protein expression, while the missense variant affected a highly conserved residue of the homeobox domain, was consistently predicted as pathogenic by bioinformatic tools, resulted in reduced protein expression and caused impaired structural stability of the homeobox domain and weaker interaction with DNA according to molecular dynamic simulations. Moreover, the nuclear localization of the mutant protein in transfected cells was significantly reduced compared to the wild-type protein. Expression studies on both patients' fibroblasts demonstrated reduced expression of *GSX2* itself, likely due to altered transcriptional self-regulation, as well as significant expression changes of related genes such as *ASCL1* and *PAX6*. Whole transcriptome analysis revealed a global deregulation in genes implicated in apoptosis and immunity, two broad pathways known to be involved in brain development. This is the first report of the clinical phenotype and molecular basis associated to basal ganglia agenesis in humans.

1 Neurogenetics Unit, IRCCS Santa Lucia Foundation, Rome, 00143, Italy
2 Neuroradiology Unit, IRCCS Istituto Giannina Gaslini, Genoa, 16147, Italy
3 Child Neuropsychiatry Unit, IRCCS Istituto Giannina Gaslini, Genoa, 16147, Italy
4 IRCCS Casa Sollievo della Sofferenza, Laboratory of Bioinformatics, San Giovanni Rotondo (FG), 71013, Italy
5 Neurosurgery Unit, IRCCS Istituto Giannina Gaslini, Genoa, 16147, Italy
6 Department of Molecular Medicine, University of Pavia, Pavia, 27100, Italy
7 Genomic and Postgenomic Lab, IRCCS Mondino Foundation, Pavia, 27100, Italy

Received December 29, 2018. Revised June 6, 2019. Accepted June 18, 2019. Advance Access publication August 14, 2019

8 Laboratory for Pediatric Brain Diseases, Rady Children's Institute for Genomic Medicine, University of California San Diego, Howard Hughes Medical Institute, La Jolla (CA), 92037, USA
9 Institute of Molecular Biology and Pathology, National Research Council, Rome, 00185, Italy
10 Department of Molecular Medicine, Sapienza University, Rome, 00161, Italy
11 Laboratory of Medical Genetics, Bambino Gesù Children's Hospital, Rome, 00146, Italy

Correspondence to: Prof. Enza Maria Valente
Department of Molecular Medicine
University of Pavia
via Forlanini 14
27100 Pavia
Italy
E-mail: enzamaria.valente@unipv.it

Keywords: basal ganglia; GSX2; homeobox; lateral ganglionic eminence; diencephalic-mesencephalic junction

Abbreviations: DMJ = diencephalic-mesencephalic junction; M/LGE = medial/lateral ganglionic eminence

Introduction

The basal ganglia are symmetrical subcortical grey nuclei at the core of the extrapyramidal system, composed by the striatum (which comprises the putamen, caudate nucleus, olfactory tubercle, and nucleus accumbens), the pallidum, the substantia nigra, and the subthalamic nucleus. These nuclei play essential roles in regulating many brain functions, including not only control of voluntary movements but also behaviour, cognition and emotion control (Obeso *et al.*, 2014). Dysfunction of the basal ganglia is associated with a wide variety of disorders with either paediatric or adult onset. These include acquired conditions (such as hypoxic-ischaemic injury, infections and iatrogenic damage, tumours), neurodegenerative disorders (such as Parkinson's, Huntington's and Wilson's diseases, as well as neurodegeneration with brain iron accumulation), and metabolic disorders (such as lysosomal storage disorders, mitochondrial disorders, organic acidurias, or gangliosidoses) (Zuccoli *et al.*, 2015). In all these conditions, basal ganglia are normally formed and then undergo acute, subacute or chronic damage, often resulting in well-recognizable imaging patterns. Conversely, congenital malformations of the basal ganglia deriving from defects of embryogenesis are very rare. The basal ganglia embryologically derive from the prosencephalon (or forebrain), the most rostral of the three vesicles originating from early patterning of the neural tube along the anterior-posterior axis. Regional identity and pattern proliferation along this axis are carefully specified by the expression of molecules along two major signalling centres, the diencephalic-mesencephalic junction (DMJ) and the midbrain-hindbrain junction (Martinez *et al.*, 1991; Nakamura *et al.*, 2005). The prosencephalon divides into telencephalon and diencephalon, and the telencephalon then separates into two domains: the pallium, which gives rise to dorsal structures such as the cerebral cortex, and the subpallium, which generates ventral structures such as the basal ganglia. In particular, the latter arise from two protrusions of the ventral telencephalon termed the medial ganglionic eminence (MGE), from which the globus pallidus originates, and the lateral ganglionic eminence (LGE), which gives rise to the caudate, the putamen and the olfactory tubercle (Smart and McSherry, 1982; Smart, 1985; Deacon *et al.*, 1994). The ganglionic eminences also represent the major source of interneurons which then migrate into the olfactory bulb and the cerebral cortex (Anderson *et al.*, 1999; Parnavelas, 2000).

Dysmorphic basal ganglia, with lack of clear separation between the caudate, putamen and globus pallidus due to the absence of various parts of the internal capsule, represent a hallmark feature of tubulinopathies, a group of autosomal dominant disorders due to mutations in tubulin family genes. Dysmorphisms are often asymmetric and occur in association with a wide range of brain malformations, including commissural abnormalities, various cortical migration defects and hypo-dysplasia of the brainstem and cerebellum (Bahi-Buisson *et al.*, 2014; Romaniello *et al.*, 2017). Another rare disorder featuring poorly delineated basal ganglia is X-linked lissencephaly with abnormal genitalia (XLAG) due to mutations in the *ARX* gene. As in tubulinopathies, the malformative pattern in this condition is complex, featuring lissencephaly, agenesis of the corpus callosum, hypoplasia of the olfactory bulbs and of the midhindbrain, and corticospinal tract anomalies (Bonneau *et al.*, 2002; Kato *et al.*, 2004; Okazaki *et al.*, 2008).

To our knowledge, neurodevelopmental disorders characterized by complete or partial agenesis of the basal ganglia, especially in the absence of cortical and/or commissural defects, are not known. A neuropathological finding of isolated basal ganglia agenesis was only reported in a 6-year-old male, with suggestion that downregulation of the *ASCL1* gene could be responsible for this defect (Sarnat, 2000); however, clinical and genetic data were not available.

Here we describe two unrelated children presenting a highly distinctive congenital brain malformation characterized by agenesis of the putamen and globi pallidi and

dysplasia of the caudate nuclei. This was associated with agenesis or hypoplasia of the olfactory bulbs and dysplasia of the DMJ, resulting in a severe phenotype of generalized dystonia, spastic tetraparesis and intellectual impairment. Both children carried homozygous pathogenic variants in the *GSX2* gene, encoding a homeobox transcription factor essential for development of the LGE.

Materials and methods

Patients and genetic studies

The two probands and their unrelated parents underwent whole-exome sequencing (WES) as part of an ongoing research project to identify the genetic basis of developmental brain defects, approved by the Ethics Committee of University of Pavia. Written informed consent was obtained according to the Declaration of Helsinki by all participating families prior entering the study. Briefly, exome capture was performed using the SureSelectXT V4 51mb Exome (Agilent Technologies) with 100-bp paired-end read sequences generated on a HiSeq2500 (Illumina). Sequences were aligned to hg19 and variants were identified and filtered as described previously (Roosing *et al.*, 2016). Mean target coverage was 80×, and >80% of bases were sequenced with a quality score above Q30.

GSX2 variants were verified by bidirectional Sanger sequencing in available family members. Potential pathogenicity was predicted using the software tools SIFT, PolyPhen-2, PROVEAN, MutationAssessor, MutationTaster and CADD. Conservation of affected residues was assessed by the Clustal Omega software. Sanger sequencing was also used to bidirectionally sequence all exons and exon-intron junctions of the *GSX2* gene in eight additional patients with DMJ dysplasia. Reference sequences were: *GSX2* gene, NM_133267.2; and GSX2 protein, NP_573574.1.

Molecular dynamics analysis

The primary protein sequence of wild-type GSX2 was obtained from UniProt (ID: Q9BZM3). The protein structure resulted from multiple alignments between several templates and the query sequence, through MODELLER v9.16. (Webb and Sali, 2014). The obtained wild-type model was mutated *in silico* through UCSC Chimera (Pettersen *et al.*, 2004), yielding a second model. The final models where embedded in boxes, extending up to 12 Å, and solvated using the TIP3P water model (Jorgensen and Madura, 1983). Additionally, *tleap* was used to add counter ions and thus to neutralize the overall charge of the models. Each model was first energy minimized and then equilibrated for ~5 ns, by a time step of 1 fs.

Molecular dynamics simulations were performed using AMBER 16 on the two equilibrated models for 30 ns by a time step of 2 fs, as reported (Case *et al.*, 2016; Biagini *et al.*, 2018).

The root-mean-square deviation of atomic positions (or simply root-mean-square deviation, RMSD) is the measure of the average distance between the atoms (usually the backbone atoms) of superimposed proteins. In this case, it was used to calculate the average distance between all heavy atoms (Cα atomic coordinates) with respect to the X-ray starting structure. Unfolded proteins usually exhibit increased RMSD values. Per-residue root-mean square fluctuation (RMSF) is a measure of the deviation over time between the positions of the Cα atomic coordinates of each residue with respect to the X-ray structure, and it was calculated to evaluate the local structure flexibility. The distance among amino acids forming the binding site for DNA and the DNA itself was calculated along the whole simulation process for the wild-type and mutant proteins. RMSF, hydrogen bonds and secondary structure content were determined with the Gromacs tools: *g_rmsf*, *g_hbond* and *do_dssp*, which are interfaces to the DSSP program (Kabsch and Sander, 1983). 3D figures and motions were generated with UCSC Chimera.

Cell cultures, plasmids, transfections and treatments

Patients' fibroblasts and HeLa cells were maintained in Dulbecco's modified Eagle medium, supplemented with 2 mM L-glutamine, 200 U/ml penicillin, 200 mg/ml streptomycin and 10% heat inactivated foetal bovine serum at 37°C in 95% humidifier air and 5% CO_2. pCMV6-AC-GSX2^{wt} was obtained from Origene Technologies. *In situ* mutagenesis was carried out at Eurofins Genomics to generate pCMV6-AC-GSX2^{Q251R} and pCMV6-AC-GSX2^{S9*}. HeLa cells were transfected with Lipofectamine® 2000 reagent (Thermo Fisher Scientific). For experiments of autophagy or proteasomal inhibition, fibroblasts were exposed to either 5 mM 3-methyladenine (3MA), 50 µM MG132, or the vehicle dimethylsulphoxide (DMSO) at the indicated times.

Immunofluorescence

Transfected HeLa cells were fixed in paraformaldehyde and coverslips were rinsed and blocked in phosphate-buffered saline with 10% bovine serum albumin prior to incubation with anti-GSX2 antibody (Novus Biologicals) overnight, followed by incubation with anti-rabbit Alexa Fluor® 555 (1:5000). Nuclei were stained with Hoechst (Thermo Fisher Scientific). Images were analysed with a confocal microscope (C2 Confocal Microscopy System). To evaluate subcellular localization of GSX2^{wt} versus GSX2^{Q251R}, the fluorescence intensity of transfected proteins in the nucleus and cytoplasm were assessed, counting 10 fields in each of three independent experiments. In particular, for each cell it was evaluated whether nuclear fluorescence signal exceeded that of cytosol or vice versa. Cells with equivalent fluorescence signals in both compartments were not counted. The relative numbers of cells with predominant nuclear or cytoplasmic fluorescent signal per total number of examined cells were calculated and expressed as a percentage.

Immunoblotting

For total extracts, cells were lysed in RIPA buffer containing protease and phosphatase inhibitors and protein extracts were quantified by Bradford assay.

For nucleus/cytoplasm fractionation, transfected HeLa cells were first suspended in a buffer containing 10 mM HEPES pH 7.9, 1.5 mM $MgCl_2$, 10 mM KCl and protease inhibitors. After centrifugation (14 000 rpm), cytoplasmic protein extracts were

isolated and then pellets were suspended in a second buffer containing 20 mM HEPES pH 7.9, 25% glycerol, 420 mM NaCl, 1.5 mM $MgCl_2$, 0.2 mM EDTA and protease inhibitors to obtain nuclear proteins. Equivalent amounts of lysates were resolved by electrophoresis through 4–20% Mini-PROTEAN TGX Gel (Bio-Rad) and probed with primary anti-GSX2 and secondary anti-rabbit-HRP antibody (Sigma Aldrich). Detection was performed by Pierce ECL Western Blotting Substrate (Thermo Fisher Scientific). Experiments were normalized by α-Tubulin or GAPDH (Sigma Aldrich), or RB (BD Bioscience). Image contrast and brightness were optimized using Adobe Photoshop CS6 (Adobe Systems Incorporated). Densitometry measurements were calculated using ImageJ Software. Original blots of all experiments are shown in the Supplementary material ('Expanded data' section).

RT-PCR

Total RNA was extracted using the High Pure RNA Isolation Kit (Roche) and then reversely transcribed with SuperScript™ II Reverse Transcriptase (Thermo Fisher Scientific). Resulting cDNAs were quantified by real-time PCR using SYBR® Green master mix on the HT-7900 platform (Thermo Fisher Scientific), to evaluate the expression levels of *GSX2* target genes *ASCL1*, *PAX6*, *DLX1*, *DLX2*, *SOX4* and *MAP2*, as well as *GSX2* itself. Primers are listed in Supplementary Table 1. The relative expression was calculated using the ΔΔCT method.

Whole transcriptome analysis

Total RNAs extracted from fibroblasts of the two patients and three controls were quantified using a Nanodrop ND-100 Spectrophotometer (Nanodrop Technologies) and a 2100 Bioanalyzer (Agilent RNA 6000 Nano Kit) to ensure a 260:280 ratio $\geqslant 1.5$ and an RNA integrity number $\geqslant 8$.

Sequencing libraries were prepared by SENSE Total RNA-Seq Library Prep Kit (Lexogen), assessed on a 2100 Bioanalyzer with a High Sensitivity assay, and sequenced on a NextSeq 500 Sequencer (Illumina). FastQ files were demultiplexed via Illumina bcl2fastq2 (v.2.17.1.14) starting from binary base call files. Mapping and quantification of transcripts were computed by STAR/RSEM software using Gencode Release 19 (GRCh37.p13) as a reference and setting the 'stranded' option. Differential expression analysis was performed using R package EBSeq2 (Leng *et al.*, 2013).

Pathway analysis

Gene set enrichment analysis was performed for coding genes. Gene Ontology (GO) enrichment analysis for biological processes, cellular components and molecular functions and a KEGG pathway analysis were conducted via enrichR web tool (Kuleshov *et al.*, 2016). GO semantics classes and pathways were considered significant for *P*-values <0.05.

Statistical analysis

Quantitative RT-PCR data and densitometric analysis are expressed as mean ± standard error. Statistical significance was evaluated by one tailed Student's *t*-test. A *P*-value of <0.05 was considered statistically significant.

Data availability

The raw data that support the findings of this study are available from the corresponding authors, upon request.

Results

Recessive variants of *GSX2* cause a complex developmental brain defect with basal ganglia agenesis

We identified two unrelated females (Patient NG4690, aged 5 years and Patient NG4687, aged 14 years) who shared a unique and highly peculiar defect of the basal ganglia, characterized by bilateral agenesis of both the putamina and the globi pallidi with normal overlying insular cortex, hypoplasia of the thalami, and dysmorphic caudate nuclei with enlarged head and small nodules of periventricular grey matter in the body and tail (Fig. 1). In addition, both children presented agenesis or hypoplasia of the olfactory bulbs, dysplasia of the DMJ characterized by hypothalamic-mesencephalic fusion and bilateral oblique linear signal anomalies (hyperintense on T_2- and hypointense on T_1-weighted images) in the middle portions of the cerebral peduncles, and abnormal course of the corticospinal tracts in the brainstem (Fig. 2). No abnormalities in distribution or calibre of the cerebellothalamic tracts were found.

Both patients were born after uneventful pregnancies and appeared to be normal at birth. Clinical features manifested in the first weeks of life with developmental delay, feeding difficulties and axial hypotonia. They progressively developed spastic quadriparesis with superimposed severe dystonic movements and postures of the limbs and trunk. They maintained eye contact, relational smile and vocalizations but were unable to speak. Detailed clinical features of each patient are described in the Supplementary material.

After WES, variants identification, annotation and filtering in the two trios, both patients were found to carry homozygous variants in the *GSX2* gene. Patient NG4690 carried the nonsense variant c.27G>A; p.(S9*), predicted to result in a truncated protein expressing only the first nine amino acids. Patient NG4687 carried the missense variant c.752A>G; p.(Q251R). This variant affected a highly conserved amino acid residue and was consistently predicted to be damaging or deleterious by all tested *in silico* predictors (Supplementary Fig. 1). Both variants segregated with the disease and were absent from all public reference databases (dbSNP, EVS, gnomAD) and from our combined in-house database including over 6000 individuals of different ethnicity.

Sanger sequencing of the coding region of *GSX2* in additional eight probands with various types of DMJ dysplasia but without basal ganglia agenesis did not reveal pathogenic variants.

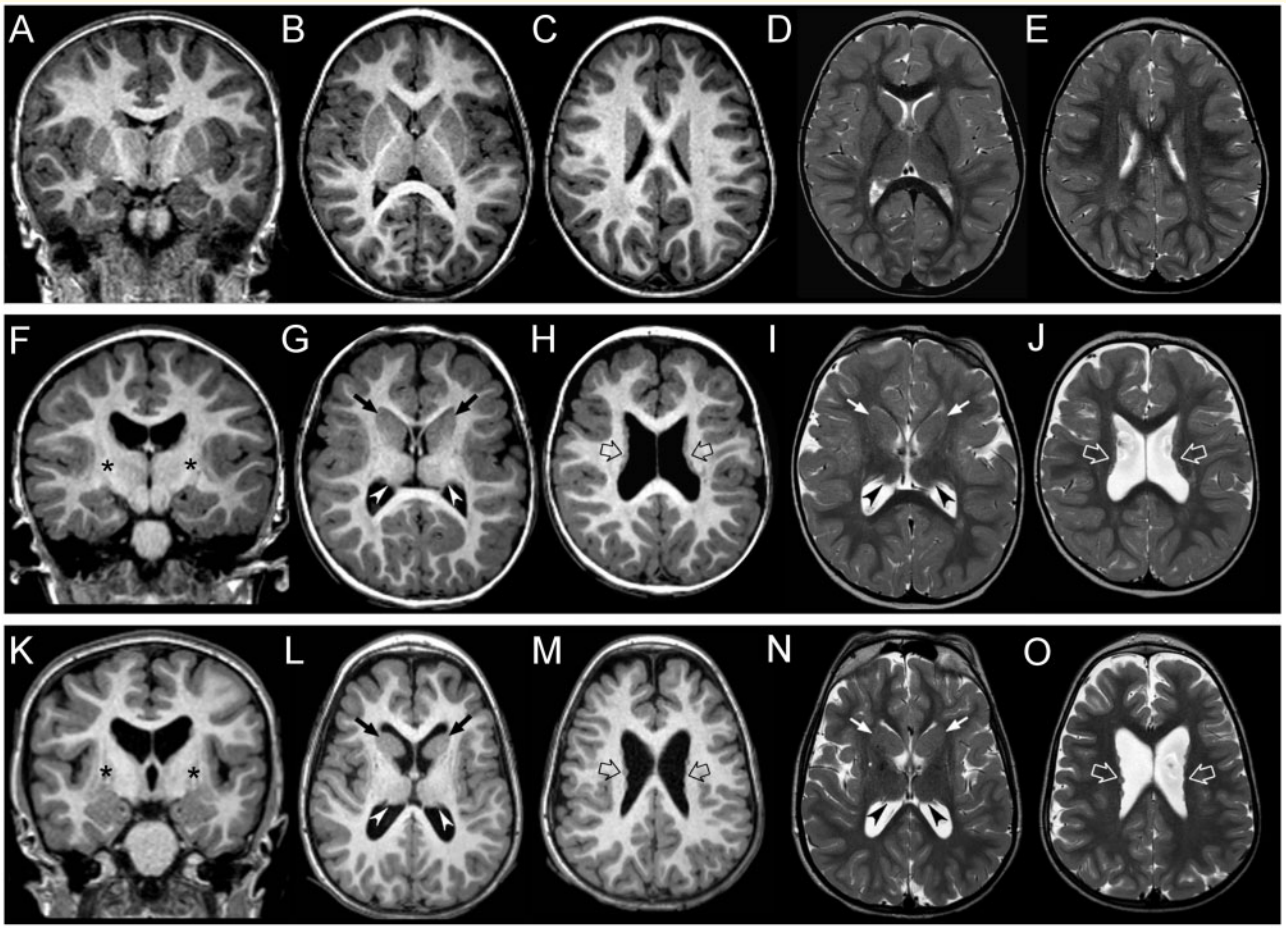

Figure 1 Brain MRI showing basal ganglia agenesis in *GSX2*-mutated patients. Coronal (**A**) and axial reformatted (**B** and **C**) 3D T_1-weighted and axial T_2-weighted (**D** and **E**) images of a control subject demonstrate the normal appearance of basal ganglia. Corresponding images performed in Patient NG4690 at 2.5 years of age (**F**–**J**) and Patient NG4687 at 10.5 years of age (**K**–**O**) reveal bilateral agenesis of the putamina and globi pallidi (black asterisks). The caudate nuclei are dysmorphic with enlarged head (small arrows) and small nodules of periventricular grey matter in the body and tail (empty arrows). Note the additional hypoplasia of the thalami (arrowheads).

The missense variant p.(Q251R) alters dynamic properties and subcellular localization of GSX2 protein

GSX2 encodes a transcription factor with a highly conserved homeobox domain, consisting of three helical regions folded into a tight globular structure that recognize and bind to DNA. The p.(Q251R) variant falls within the third helix of the homeobox domain, which is the most important region for DNA recognition and binding. To assess the pathogenicity of this variant, we obtained a 3D model of the GSX2 protein and then performed several molecular dynamics analyses to compare structural stability and flexibility, long range interactions between residues, and distance between non-bonded entities in the contact region of the homeodomain-DNA complex in the wild-type versus the mutant protein. According to molecular dynamics simulations, the presence of the missense variant resulted in reduced stability and increased structural flexibility of the GSX2 homeodomain, particularly in helix III (Fig. 3A and B). In line with these findings, in the mutant protein the distances between non-bonded entities in the contact region of the homeodomain–DNA complex were largely floating and nearly always greater than those measured for the wild-type protein, in which conversely, the distance remained quite uniform throughout the simulation (Fig. 3C).

Previous molecular dynamics simulations performed on homologous proteins (Zhao *et al.*, 2006) allowed identifying a number of water-mediated hydrogen bonds between residue Q50 (corresponding to Q251 in the GSX2 protein) and the DNA. Recent surveys of structural data on protein-protein and protein-DNA recognition sites have indicated that water is present in abundance at the interface, and the analysis of different high-resolution structures allowed the identification of at least as many water-mediated interactions as direct hydrogen bonds or salt bridges

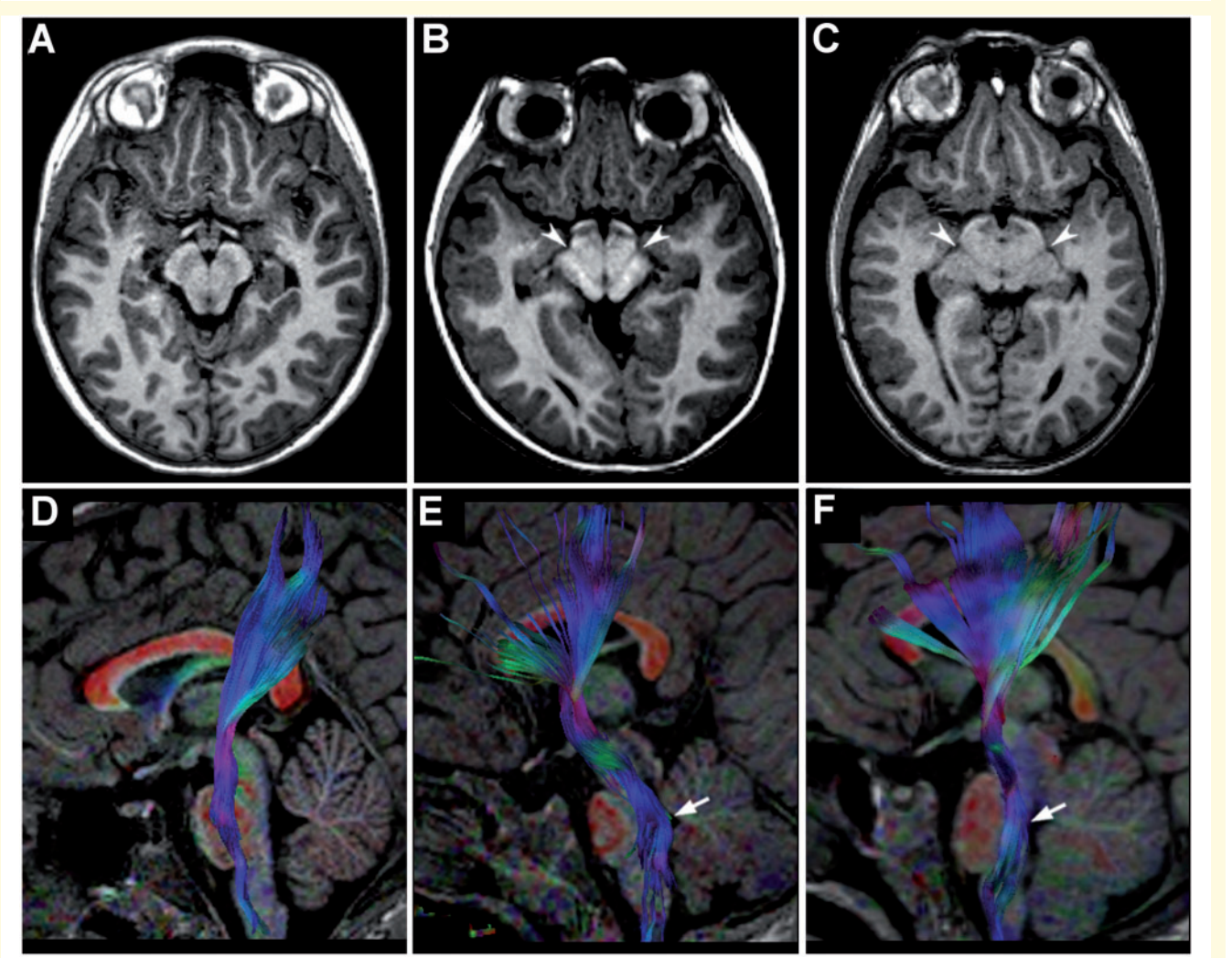

Figure 2 Brain MRI showing DMJ and corticospinal tracts abnormalities in patients with *GSX2* mutations. Axial reformatted 3D turbo field echo (TFE) T_1-weighted image in a healthy control (**A**) and in Patients NG4690 and NG4687 (**B** and **C**). Both patients present abnormal contour of the midbrain with fusion of the hypothalamus and midbrain and bilateral oblique linear hypointense stripes (arrowheads). Sagittal fractional anisotropy colour directional maps fused with 3D/TFE T_1-weighted images and with motor tractography in a healthy control (**D**) and in Patients NG4690 and NG4687 (**E** and **F**). Images from patients reveal abnormal dorsal course of the corticospinal tracts at the level of the pons (arrows).

(Janin, 1999). Thus, interfacial water may play an important role in mediating contact between protein residues and the corresponding DNA bases due to the presence of phosphate groups on the DNA side and of positively charged groups on the protein side. Interestingly, in wild-type GSX2 the side chain of Q251 allows water-mediated hydrogen bonds to establish, whereas these cannot be formed in the presence of the mutant arginine (Fig. 3D). Taken together, the results of molecular dynamics studies consistently suggest that the p.(Q251R) variant may significantly weaken the interaction between the homeobox domain and DNA.

To evaluate the disruptive effect of this missense variant on the protein function further, we overexpressed either wild-type or mutant GSX2 in HeLa cells and evaluated their subcellular localization by immunofluorescence. Wild-type GSX2 localized mainly in the cellular nuclei and to a much lesser extent in the cytoplasm, while nuclear localization was significantly reduced for mutant GSX2, which was more abundant in the cytoplasm (Fig. 4A). This observation was confirmed by nucleus-cytoplasm fractionation experiments, showing an inverted ratio of the mutant versus the wild-type protein (Fig. 4B).

Both variants impair transcriptional regulatory activity of the GSX2 protein

Next, we analysed by western blotting the expression levels of endogenous GSX2 protein in patients' fibroblasts. We failed to detect any protein expression in cells harbouring the nonsense variant p.(S9*), while GSX2 carrying the

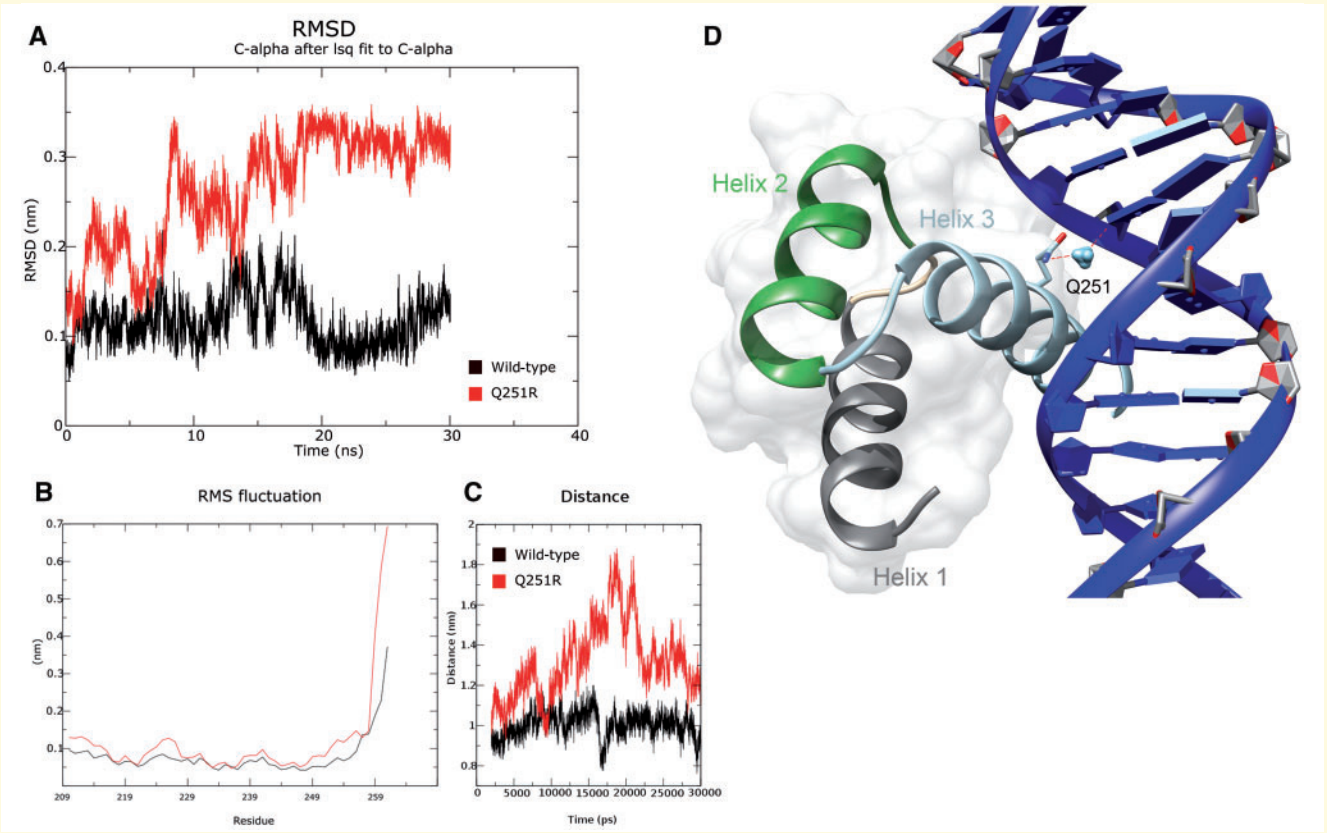

Figure 3 Molecular dynamics of wild-type and mutant GSX2. (**A**) Instantaneous root-mean-square deviation (RMSD) of all GSX2 heavy atoms. (**B**) Root-mean-square fluctuations (RMSF) of residue coordinates during simulations. (**C**) Distance between amino acids forming the binding site for DNA and the DNA itself. Wild-type and mutant GSX2 are coloured in black and red, respectively. (**D**) 3D structure of the homeobox domain of the GSX2 protein in complex with the DNA; location of $GSX2^{Q251}$ and water bridge bonds (red dashed lines) with the DNA, which do not form in presence of the $GSX2^{Q251R}$ mutation.

p.(Q251R) missense variant was expressed, although at significantly lower levels than the wild-type protein in control cells (Supplementary Fig. 2A). To explore whether this could depend on enhanced degradation of the mutant protein, we evaluated protein expression levels upon treatment of fibroblasts with either MG132 or 3MA, to block the ubiquitin-proteasome or the autophagy pathway, respectively. Upon proteasomal blockage, the wild-type protein significantly increased, demonstrating that GSX2 is physiologically degraded through this pathway. Interestingly, the levels of $GSX2^{Q251R}$ remained unchanged after MG132 treatment, suggesting that either the mutant protein acquired conformational changes that made it less prone to be degraded by the proteasome, or that the protein levels were too low to trigger its degradation (Supplementary Fig. 2B). Conversely, both wild-type and mutant protein levels remained unchanged after 3MA treatment, indicating that GSX2 is not degraded through the autophagy pathway (Supplementary Fig. 2C). Taken together, these results indicate that the reduced levels of $GSX2^{Q251R}$ in patient's fibroblasts do not depend on increased protein degradation.

We next measured by quantitative RT-PCR the levels of *GSX2* mRNA in patients' fibroblasts. Surprisingly, both mutant lines had *GSX2* mRNA levels that were halved compared to control fibroblasts (Fig. 5). On one hand, this result excluded nonsense-mediated decay of the transcript carrying the nonsense variant c.27G>A. This mRNA is predicted to encode for a truncated protein of only nine amino acid residues, which likely could not be detected by the anti-GSX2 antibody. On the other hand, the interesting observation that *GSX2* mRNA levels are significantly reduced in both patients suggests a mechanism of autoregulation of transcription by the GSX2 protein itself, as it was already proven for many transcription factors (Kielbasa and Vingron, 2008; Crews and Pearson, 2009).

In light of the results generated by dynamic modelling, subcellular localization and expression studies, we next sought to verify the impact of both variants on the transcriptional regulator activity of GSX2. To this aim, we assessed the expression levels of the two genes that are known to be positively (*ASCL1*) or negatively (*PAX6*) regulated by *GSX2* (Toresson *et al.*, 2000; Wang *et al.*, 2009). Moreover, we also monitored the levels of two

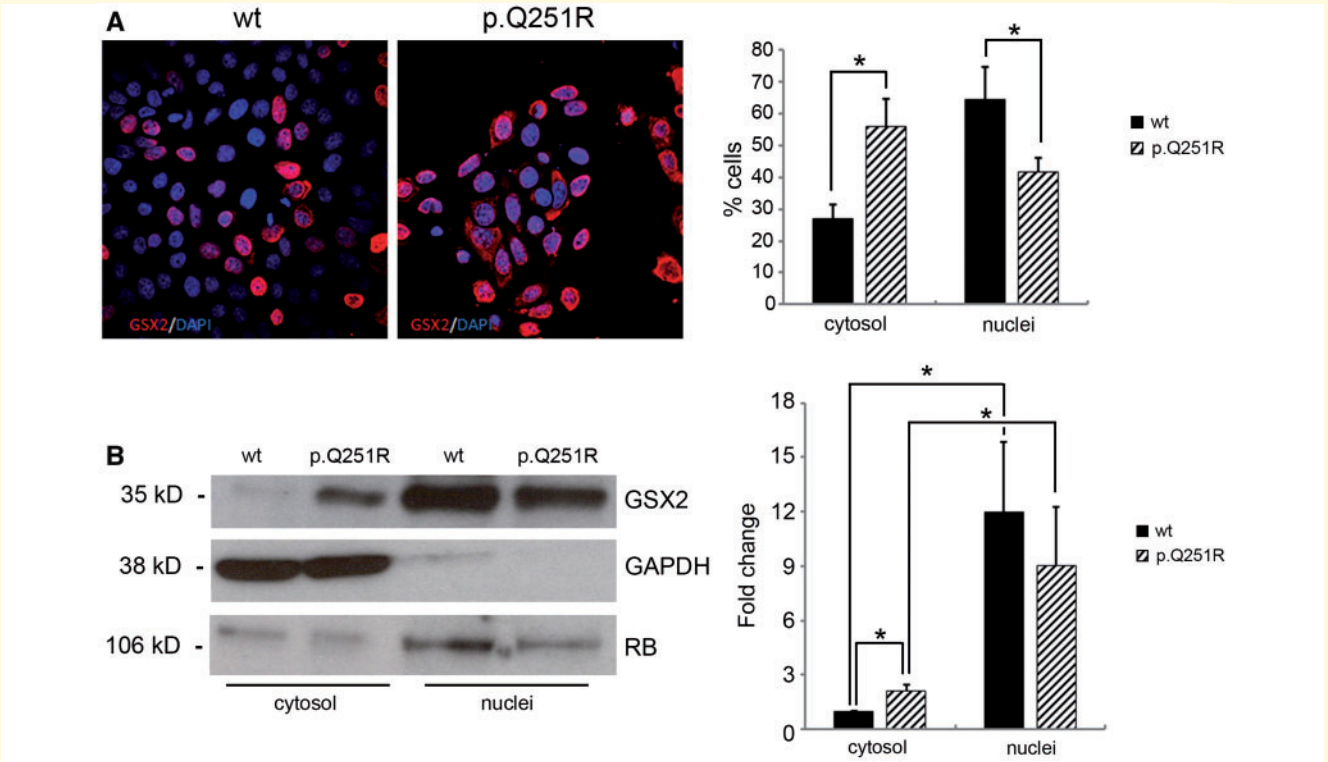

Figure 4 Intracellular localization of wild-type and mutant GSX2. (**A**) Immunofluorescence showing GSX2 intracellular localization. Transfected HeLa cells were stained with anti-GSX2 (red) and DAPI (blue). Wild-type GSX2 localizes predominantly in the nuclei (64 ± 4% of counted cells versus 27 ± 10% with predominant cytoplasmic localization), while mutant GSX2^{Q251R} localizes both in the nuclei (56 ± 4%) and cytoplasm (42 ± 9%). (**B**) Nucleus-cytoplasm fractionation experiments and related densitometries of western blotting, with cytoplasmic wild-type protein set at 1, demonstrate that sublocalization is predominantly nuclear for the wild-type protein (12.0 ± 3.83) while, compared to the wild-type, the mutant protein shows increased cytoplasmic (2.12 ± 0.36) and reduced nuclear (9.02 ± 3.25) localization. Results are shown as mean ± standard error of three (**A**) or four (**B**) independent experiments. *$P \leqslant 0.05$.

additional genes (*DLX1* and *DLX2*) that act downstream of *ASCL1* in the same transcriptional network (Liu *et al.*, 2017). As expected, in both patients' fibroblasts, *ASCL1* levels were significantly reduced (fold-change 0.2–0.4) while *PAX6* levels were markedly elevated (fold-change ~8) compared to control fibroblasts. Interestingly, *DLX1* and *DLX2* levels were also upregulated, more evidently for *DLX1* (fold-change ~10) (Fig. 5), confirming that GSX2 loss of function results in a global deregulation of the expression of downstream genes.

To confirm these findings and to obtain a global view of differentially expressed mRNA transcripts, we performed a whole transcriptome analysis from fibroblasts of the two patients and three healthy controls. Overall, we identified a small number of upregulated genes while many more genes were downregulated in the two patients (Supplementary Table 2). Data analysis showed a common profile of differentially expressed genes shared by the two patients compared to controls (Fig. 6A and B). Besides confirming previous results, whole transcriptome analysis showed a significant downregulation of other genes potentially related to *GSX2*, such as *SOX4* and *MAP2*, which was confirmed by real-time PCR (Fig. 6C and D).

The complete list of significantly deregulated genes in patients' versus control fibroblasts is presented in Supplementary material, File 2. Analysis of these genes and their related biological processes highlighted a downregulation of genes implicated in cellular senescence and apoptosis, and a global deregulation (with many upregulated transcripts) of genes implicated in inflammation and immunity (Supplementary Fig. 3).

Discussion

Homeobox genes represent an evolutionary conserved family of genes that play essential roles in regulating embryonic development. While Hox genes reside in clusters and their involvement in brain development is restricted to the hindbrain (Keynes and Krumlauf, 1994), several non-clustered homeobox genes are expressed in the developing forebrain and midbrain and are responsible for pattern formation of these regions (Rubenstein and Puelles, 1994). In mice, *Gsx2* was first identified along with its closely related *Gsx1*, as two non-clustered homeobox genes homologues of the *Drosophila ind* gene,

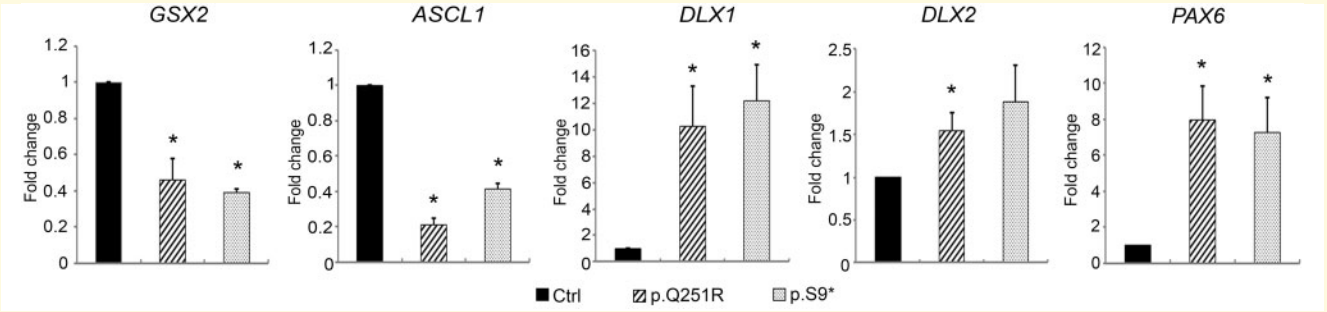

Figure 5 Impact of *GSX2* mutations on the expression levels of downstream genes. mRNA levels of *GSX2* and downstream genes *ASCL1*, *PAX6*, *DLX1* and *DLX2* in fibroblasts from patients and controls. *GSX2* and *ASCL1* levels are significantly reduced, while expression levels of *PAX6*, *DLX1* and *DLX2* are increased in mutated cells compared to control cells. Results are shown as mean ± standard error of at least three independent experiments; $*P \leqslant 0.05$.

encoding a protein essential for dorsal-ventral cell fate specification in the *Drosophila* nervous system (Singh *et al.*, 1991; Corbin *et al.*, 2000). Early studies in the developing murine brain showed that both *Gsx1* and *Gsx2* are similarly expressed in the developing MGE and diencephalon, as well as in restricted areas of the midbrain and hindbrain (Hsieh-Li *et al.*, 1995; Valerius *et al.*, 1995), while *Gsx2* alone is much more prevalent in the developing LGE, especially during early telencephalic development (Corbin *et al.*, 2000). Within these regions, *Gsx2* is highly expressed in neural progenitors, where it promotes neuronal differentiation while negatively regulating the formation of oligodendrocyte precursors (Chapman *et al.*, 2013).

Here, we report two children presenting a unique complex malformation of the basal ganglia and the DMJ, caused by homozygous loss of function variants of the *GSX2* homeobox gene. The nonsense variant results in lack of expression of the truncated protein, while the protein harbouring the missense variant is expressed at reduced levels, is retained in the cytosol, and shows altered dynamic properties which likely hamper its binding to DNA. As a consequence, fibroblasts from both affected children showed a deregulation of *GSX2* downstream genes, with upregulation of *PAX6*, *DLX1* and *DLX2* and downregulation of *ASCL1* and *GSX2* itself.

Strikingly, the transcriptional defects as well as the neuroimaging phenotype observed in our patients closely mirror the developmental abnormalities seen in *Gsx2* knock-out mice. *In situ* hybridization experiments in these animal models showed that *Gsx2* is essential for the early expression of several genes involved in GABAergic specification and differentiation of the LGE (Szucsik *et al.*, 1997; Corbin *et al.*, 2000). In particular, the lack of *Gsx2* was found to increase the expression of dorsal telencephalic genes such as *Pax6*, which is involved in the differentiation of both forebrain and midbrain, while impairing the expression of ventral regulators such as *Ascl1* (also known as Mash1) within the LGE (Yun *et al.*, 2001). Unexpectedly, *DLX1* and *DLX2* showed an opposite trend in our patients' fibroblasts compared to the *Gsx2* knock-out mice, in which their expression levels were selectively downregulated within the LGE while remaining unaltered in the MGE and other brain areas (Szucsik *et al.*, 1997). Yet, it must be noted that these two genes are known to be negatively regulated by *Ascl1*, as they are both overexpressed in the ventricular zone of *Ascl1*/Mash1 knock-out mice (Casarosa *et al.*, 1999). Thus, it can be speculated that in *GSX2*-mutated fibroblasts, the repressed *ASCL1* levels may play a more relevant role than *GSX2* itself in modulating *DLX1* and *DLX2*, which therefore appear upregulated compared to controls, albeit their expression levels in the developing brain of *GSX2*-mutated patients remain unpredictable.

Whole transcriptome analysis in patients' fibroblasts further disclosed the downregulation of genes more distantly related to *GSX2*, such as *SOX4* and *MAP2*. *SOX4*, along with *SOX11* and *SOX12*, form the group C of SRY-related (SOX) transcription factors, and play additive and redundant roles in multiple developmental pathways, including neurogenesis and skeletogenesis. In particular, during mouse cerebral cortex formation, *Sox4* is highly expressed in intermediate progenitor cells where it regulates their survival and maintenance (Chen *et al*, 2015). *MAP2* encodes a protein of the microtubule-associated protein family involved in microtubule assembly, which represents an essential step in neurogenesis. It is highly expressed in foetal brain, mainly in the cortex, amygdala, hypothalamus and basal ganglia. In mouse, *Map2* expression is enriched in dendrites, where it likely stabilizes dendritic shape during neuronal development along with other MAP family proteins (Tucker, 1990). Several additional genes implicated in embryonic brain development were significantly downregulated in both patients' fibroblasts. Among these are *SPON1*, *SH3GL2*, and *CADM1*, encoding for three proteins (spondin, endophilin A1 and cell adhesion molecule 1) involved in axonal and dendritic outgrowth and guidance, as well as *SFRP2* and *WISP2*, encoding for two proteins (secreted frizzled related protein 2 and WNT1 inducible signalling pathway protein 2) related to the Wnt pathway.

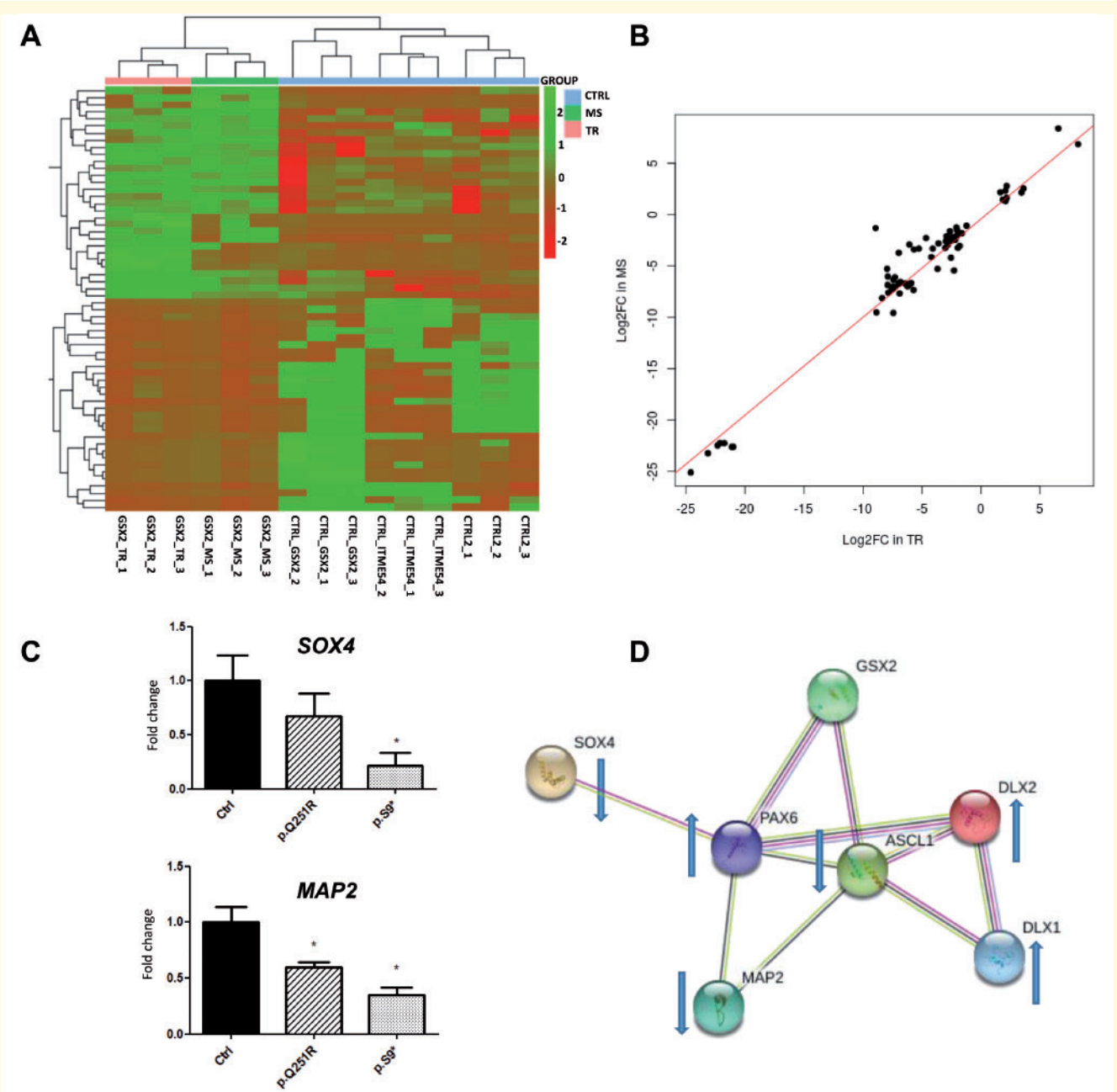

Figure 6 Whole transcriptome analysis. (**A**) Heat map of log-normalized mRNA expression counts for *GSX2* p.S9* (green) and p.Q251R (pink) versus controls (light blue), built using the top 60 differentially expressed mRNAs. The image shows a common deregulation between *GSX2*-mutated patients that clearly differ from healthy controls. (**B**) Common genes differentially expressed in both mutant cell lines share a very similar behaviour in terms of log2FC over controls. Black dots represent log2FC values in p.S9* (*x*-axis) and p.Q251R group (*y*-axis). Red solid line is the regression line, with a coefficient of determination $R^2 = 0.95$. (**C**) Real time PCR of *SOX4* and *MAP2* genes, confirming a significant downregulation in patients' fibroblasts. (**D**) String analysis of *GSX2*-related pathways showing the interaction among proteins encoded by core deregulated genes.

Besides neurodevelopmental genes, whole transcriptome study and related pathway analysis in the two patients' fibroblasts revealed a downregulation of genes related to cellular senescence and apoptosis and, more remarkably, a global deregulation of genes implicated in pathways related to immunity and inflammation, such as chemokine receptors and ligands, cytokine receptors, complement subunits and tumour necrosis factor-related proteins (Supplementary material, File 2). These findings are particularly intriguing in light of recent evidences pointing out to a central role for microglia, the specialized resident immune cells of the CNS, in orchestrating many of the complex processes taking place during embryonic brain development. These include regulation of neurogenesis both by

direct phagocytosis of progenitor cells and by control of programmed cell death, regulation of brain wiring and modulation of synaptic formation and pruning (Frost *et al.*, 2016). In particular, microglial control of neuronal death and survival is known to be mediated by the release of growth factors, interleukins and cytokines (Mosser *et al.*, 2017; Thion *et al.*, 2018); it can be speculated that the lack of functional *GSX2* in the developing brain of our patients could have resulted in a global deregulation of microglia-related functioning, with a cascade effect eventually affecting not only the development of structures directly deriving from the LGE, but also of the CNS at large, thus contributing to the severe neurological phenotype observed in both children. This hypothesis, however, requires validation, as currently there are no specific studies on microglia or other immune-related cells in *Gsx2* animal models.

Gsx2 knock-out mice are viable until birth but die within the first 24 h of postnatal life due to prolonged episodes of central apnoea. Upon histological analysis of the brain at developmental time points E12.5 to E17.5, the most striking abnormality is a significant reduction in size of the LGE, which persists at later time points (Szucsik *et al.*, 1997). Although less severe, patterning defects are also found in the medial and caudal ganglionic eminences. Moreover, these mice show abnormal migration of interneurons in the olfactory bulb, while migration to the cerebral cortex seems to be largely unaffected (Corbin *et al.*, 2000). In addition to the defects in LGE development, the area postrema and the adjacent solitary tract nucleus also failed to develop. These two hindbrain structures are relevant for the control of cardiorespiratory physiology and could be implicated in the prolonged apnoea experienced by these animals early in life (Szucsik *et al.*, 1997).

Similar to the animal model, both *GSX2*-mutated patients presented agenesis or dysgenesis of the structures derived from the lateral and median ganglionic eminences, including the putamina, the globi pallidi, the caudate nuclei and the olfactory bulbs. Conversely, while it is known that *Gsx2* is expressed in the developing ventral thalamus of mice (Corbin *et al.*, 2000), data on thalamic expression of this gene in humans are lacking, and it remains unclear if the thalamic hypoplasia observed in our patients is a primary process or the consequence of altered basal ganglia-thalamo-cortical connectivity. The observed complex malformation well explains the clinical picture, which is dominated by severe dyskinetic movements and generalized dystonic postures, albeit both patients failed to present the episodes of central apnoea which are lethal for the knock-out mice.

To date, congenital dysmorphisms of the basal ganglia have been reported in patients with either tubulinopathies or XLAG (Bonneau *et al.*, 2002; Kato *et al.*, 2004; Okazaki *et al.*, 2008; Bahi-Buisson *et al.*, 2014). Tubulins represent a protein family essential for assembly and functioning of microtubules, dynamic cytoskeletal components that are crucial to sustain the extensive migration of neurons during brain development (Jaglin and Chelly, 2009). Despite the high degree of homology among distinct tubulins and their potential functional redundancy, distinct tubulin-mutant animal models consistently show robust and widespread neuronal migratory defects (Belvindrah *et al.*, 2017). Of note, basal ganglia anomalies in *TUBB4A* mutations are related to an atrophic process in the context of a hypomyelination disorder (Simons *et al.*, 2013), while in other tubulinopathies they are secondary to the abnormal course of the white matter tracts in the anterior limbs of internal capsules (Mutch *et al.*, 2016). In both cases, they are secondary processes rather than the result of an impaired basal ganglia formation. *ARX* encodes a transcription factor of the Aristaless-related paired-class homeobox family widely expressed in the forebrain, that is specifically involved in the proliferation, radial and tangential migration, and differentiation of GABAergic interneurons from the ganglionic eminences to the intermediate and subventricular zones and then to the cortical plate. *Arx* mutant mice showed periventricular accumulation of immature neurons in both the LGE and MGE, with strong impairment of both tangential migration towards the cortex and striatum and radial migration to the striatum and globus pallidus (Kitamura *et al.*, 2002; Colombo *et al.*, 2007). The widespread function of tubulins and *ARX* in the development of several embryonic brain structures explains the complex developmental defects associated with mutations in these genes, in which basal ganglia dysmorphisms are part of a wider, severe spectrum of cortical, callosal and midbrain-hindbrain anomalies.

In addition to the basal ganglia defects, *GSX2*-mutated patients showed hypothalamic-mesencephalic fusion, representing a peculiar form of DMJ dysplasia. At difference from defects of the midbrain-hindbrain junction, dysplasia of the DMJ still remains poorly understood, and only few patients have been reported to date. Barkovich and coworkers first described three sporadic subjects presenting with midbrain enlargement, dorsoventral midline hyperintensity, and pontocerebellar hypoplasia likely due to a posterior to anterior transformation at the level of the DMJ (Barkovich *et al.*, 2007, 2009). In 2012, Zaki and colleagues described six children from three consanguineous Egyptian families with a novel malformation termed 'DMJ dysplasia' characterized by a peculiar DMJ malformation with butterfly-like contour of the midbrain on MRI axial sections; additional features were supratentorial ventriculomegaly of variable degree, commissural abnormalities and lack of identifiable corticospinal tracts (Zaki *et al.*, 2012). In 2016, we reviewed the MRI studies of 445 patients with brainstem malformations, and identified anomalies of the DMJ in 12, including the two patients reported in this study (Severino *et al.*, 2016). In some cases, we observed a complete fusion between the hypothalamus and the midbrain, leading to dorsoventral enlargement and abnormal contour of the midbrain on axial planes (variably associated to midbrain ventral cleft, ventriculomegaly, pontocerebellar hypoplasia, and abnormalities of the corticospinal tracts, commissures, basal

ganglia, and olfactory bulbs), while others had a milder phenotype, with incomplete cleavage between the thalami and the mesencephalon on the sagittal plane, associated with midbrain and cerebellar vermis hypoplasia. These data suggest that the spectrum of DMJ patterning defects is wide and might be found in a heterogeneous group of genetic conditions that need to be further stratified according to clinical and other neuroimaging features.

Recently, biallelic loss of function variants in the protocadherin 12 gene (*PCDH12*), encoding a cell surface protein promoting cell adhesion and neurite outgrowth, have been identified in 14 patients with DMJ dysplasia from eight independent families. Patients presented a peculiar clinical-radiological phenotype characterized by progressive microcephaly, severe cognitive impairment, dysmorphic facies, variable spasticity and epilepsy, DMJ dysplasia with midbrain ventral cleft, callosal hypoplasia, and in most cases also calcifications (Guemez-Gamboa *et al.*, 2018). Of note, *PCDH12* mutations were found in two of the three families originally described (Zaki *et al.*, 2012), while no pathogenic variants were identified in the third family with a different phenotype of massively dilated lateral ventricles, further supporting the hypothesis of different genetic mechanisms underlying DMJ disorders. In the present study, the two subjects carrying *GSX2* mutations present a distinct anomaly of the DMJ, characterized by abnormal midbrain morphology on axial plane with bilateral oblique signal alterations at the level of the cerebral peduncles (Fig. 2). Sequencing of *GSX2* in eight additional patients with other types of DMJ dysplasia and without basal ganglia agenesis failed to identify pathogenic variants, suggesting a relatively tight genotype-phenotype correlation. Moreover, we failed to identify biallelic *GSX2* pathogenic variants by WES in our extended cohort of over 10 000 children with either spastic tetraparesis, movement disorders or intellectual disability, and additional mutated cases were not reported in online databases aimed at sharing phenotypic and genotypic data (such as Matchmaker), suggesting that *GSX2* mutations are very rare and associate with a highly specific neuroradiological phenotype.

Interestingly, fibroblasts from both *GSX2*-mutated patients showed increased expression levels of *PAX6*, which is involved in the differentiation of both forebrain and midbrain (Yun *et al.*, 2001; Spieler *et al.*, 2004), and it is intriguing to speculate that disruption of the developmental cascade involving *GSX2* and *PAX6* may specifically interfere with DMJ positioning and functioning. Animal models have shown that the formation and location of the DMJ depend on a fine-tuned interplay among several genes (including *Pax6*, *En1*, and *Pax2*), orchestrated by *Fgf8* expression (Nakamura *et al.*, 2005). Finally, we noticed in both patients an abnormally dorsalized course of the corticospinal tracts at the level of the pons (Fig. 2). Although the cause of this abnormality is not clear, we can speculate that the overexpression of *PAX6* might eventually cause axon guidance defects of the corticospinal tracts, as this gene was found to play additional important roles in axonal pathfinding during CNS development (Mastick *et al.*, 1997; Georgala *et al.*, 2011).

In conclusion, we report the first genetic cause responsible for basal ganglia agenesis in humans. We demonstrate that loss of function of *GSX2* may not be lethal but leads to an abnormal development of both LGE and MGE basal ganglia derivatives, associated with a severe hyperkinetic neurological phenotype.

Acknowledgements

We thank the patients and their family for their participation in this study.

Funding

This work was supported by grants from the European Research Council (ERC Starting Grant 260888 to E.M.V.), the Italian Ministry of Health (NET-2013–02356160 to E.M.V. and Ricerca Corrente 2018 RC18DSCOMU to T.M.), the Fondazione Mondino (5 per mille grant year 2016 to E.M.V. and C.C.), the Amber Project and NVIDIA Corporation (to T.M.), the National Institutes of Health (R01NS041537, R01NS048453, R01NS052455, P01HD070494, P30NS047101 to J.G.G.), the Howard Hughes Medical Institute and Simons Foundation (to J.G.G.). This research was also supported by a Grant of the Italian Ministry of Education, University and Research (MIUR) to the Department of Molecular Medicine of the University of Pavia under the initiative 'Dipartimenti di Eccellenza (2018–2022)'. This publication is distributed under the terms of open access policies implemented by the the Italian Ministry of Education, University and Research (MIUR).

Competing interests

The authors report no competing interests.

Supplementary material

Supplementary material is available at *Brain* online.

References

Anderson S, Mione M, Yun K, Rubenstein JL. Differential origins of neocortical projection and local circuit neurons: role of Dlx genes in neocortical interneuronogenesis. Cereb Cortex 1999; 9: 646–54.

Bahi-Buisson N, Poirier K, Fourniol F, Saillour Y, Valence S, Lebrun N, et al. The wide spectrum of tubulinopathies: what are the key features for the diagnosis? Brain 2014; 137: 1676–700.

Barkovich AJ, Millen KJ, Dobyns WB. A developmental classification of malformations of the brainstem. Ann Neurol 2007; 62: 625–39.

Barkovich AJ, Millen KJ, Dobyns WB. A developmental and genetic classification for midbrain-hindbrain malformations. Brain 2009; 132: 3199–230.

Belvindrah R, Natarajan K, Shabajee P, Bruel-Jungerman E, Bernard J, Goutierre M, et al. Mutation of the alpha-tubulin Tuba1a leads to straighter microtubules and perturbs neuronal migration. J Cell Biol 2017; 216: 2443–61.

Biagini T, Chillemi G, Mazzoccoli G, Grottesi A, Fusilli C, Capocefalo D, et al. Molecular dynamics recipes for genome research. Brief Bioinform 2018; 19: 853–62.

Bonneau D, Toutain A, Laquerriere A, Marret S, Saugier-Veber P, Barthez MA, et al. X-linked lissencephaly with absent corpus callosum and ambiguous genitalia (XLAG): clinical, magnetic resonance imaging, and neuropathological findings. Ann Neurol 2002; 51: 340–9.

Casarosa S, Fode C, Guillemot F. Mash1 regulates neurogenesis in the ventral telencephalon. Development 1999; 126: 525–34.

Case DA, Betz RM, Cerutti DS, Cheatham TE, Darden TA, Duke RE, et al. AMBER. San Francisco: University of California; 2016. http://ambermd.org/doc12/Amber16.pdf

Chapman H, Waclaw RR, Pei Z, Nakafuku M, Campbell K. The homeobox gene *Gsx2* controls the timing of oligodendroglial fate specification in mouse lateral ganglionic eminence progenitors. Dev Stem Cells 2013; 140: 2289–98.

Chen C, Lee GA, Pourmorady A, Sock E, Donoghue MJ. Orchestration of neuronal differentiation and progenitor pool expansion in the developing cortex by SoxC genes. J Neurosci 2015; 35: 10629–42.

Colombo E, Collombat P, Colasante G, Bianchi M, Long J, Mansouri A, et al. Inactivation of Arx, the murine ortholog of the X-linked lissencephaly with ambiguous genitalia gene, leads to severe disorganization of the ventral telencephalon with impaired neuronal migration and differentiation. J Neurosci 2007; 27: 4786–98.

Corbin JG, Gaiano N, Machold RP, Langston A, Fishell G. The Gsh2 homeodomain gene controls multiple aspects of telencephalic development. Development 2000; 127: 5007–20.

Crews ST, Pearson JC. Transcriptional autoregulation in development. Curr Biol 2009; 19: R241–6.

Deacon TW, Pakzaban P, Isacson O. The lateral ganglionic eminence is the origin of cells committed to striatal phenotypes: neural transplantation and developmental evidence. Brain Res 1994; 668: 211–9.

Frost JL, Schafer DP. Microglia: architects of the developing nervous system. Trends Cell Biol 2016; 26: 587–97.

Georgala PA, Manuel M, Price DJ. The generation of superficial cortical layers is regulated by levels of the transcription factor Pax6. Cereb Cortex 2011; 21: 81–94.

Guemez-Gamboa A, Caglayan AO, Stanley V, Gregor A, Zaki MS, Saleem SN, et al. Loss of protocadherin-12 leads to diencephalic-mesencephalic junction dysplasia syndrome. Ann Neurol 2018; 84: 638–47.

Hsieh-Li HM, Witte DP, Szucsik JC, Weinstein M, Li H, Potter SS. Gsh-2, a murine homeobox gene expressed in the developing brain. Mech Dev 1995; 50: 177–86.

Jaglin XH, Chelly J. Tubulin-related cortical dysgeneses: microtubule dysfunction underlying neuronal migration defects. Trends Genet 2009; 25: 555–66.

Janin J. Wet and dry interfaces: the role of solvent in protein-protein and protein-DNA recognition. Structure 1999; 7: R277–9.

Jorgensen WL, Madura JD. Solvation and conformation of methanol in water. J Am Chem Soc 1983; 105: 1407–13.

Kabsch W, Sander C. Dictionary of protein secondary structure: pattern recognition of hydrogen-bonded and geometrical features. Biopolymers 1983; 22: 2577–637.

Kato M, Das S, Petras K, Kitamura K, Morohashi K, Abuelo DN, et al. Mutations of ARX are associated with striking pleiotropy and consistent genotype-phenotype correlation. Hum Mutat 2004; 23: 147–59.

Keynes R, Krumlauf R. Hox genes and regionalization of the nervous system. Annu Rev Neurosci 1994; 17: 109–32.

Kielbasa SM, Vingron M. Transcriptional autoregulatory loops are highly conserved in vertebrate evolution. PLoS One 2008; 3: e3210.

Kitamura K, Yanazawa M, Sugiyama N, Miura H, Iizuka-Kogo A, Kusaka M, et al. Mutation of ARX causes abnormal development of forebrain and testes in mice and X-linked lissencephaly with abnormal genitalia in humans. Nat Genet 2002; 32: 359–69.

Kuleshov MV, Jones MR, Rouillard AD, Fernandez NF, Duan Q, Wang Z, et al. Enrichr: a comprehensive gene set enrichment analysis web server 2016 update. Nucleic Acids Res 2016; 44: W90–7.

Leng N, Dawson JA, Thomson JA, Ruotti V, Rissman AI, Smits BM, et al. EBSeq: an empirical Bayes hierarchical model for inference in RNA-seq experiments. Bioinformatics 2013; 29: 1035–43.

Liu YH, Tsai JW, Chen JL, Yang WS, Chang PC, Cheng PL, et al. Ascl1 promotes tangential migration and confines migratory routes by induction of Ephb2 in the telencephalon. Sci Rep 2017; 7: 42895.

Martinez S, Wassef M, Alvarado-Mallart RM. Induction of a mesencephalic phenotype in the 2-day-old chick prosencephalon is preceded by the early expression of the homeobox gene en. Neuron 1991; 6: 971–81.

Mastick GS, Davis NM, Andrew GL, Easter SS Jr. Pax-6 functions in boundary formation and axon guidance in the embryonic mouse forebrain. Development 1997; 124: 1985–97.

Mosser CA, Baptista S, Arnoux I, Audinat E. Microglia in CNS development: Shaping the brain for the future. Progr Neurobiol 2017; 149: 1–20.

Mutch CA, Poduri A, Sahin M, Barry B, Walsh CA, Barkovich AJ. Disorders of microtubule function in neurons: imaging correlates. AJNR Am J Neuroradiol 2016; 37: 528–35.

Nakamura H, Katahira T, Matsunaga E, Sato T. Isthmus organizer for midbrain and hindbrain development. Brain Res Rev 2005; 49: 120–6.

Obeso JA, Rodriguez-Oroz MC, Stamelou M, Bhatia KP, Burn DJ. The expanding universe of disorders of the basal ganglia. Lancet 2014; 384: 523–31.

Okazaki S, Ohsawa M, Kuki I, Kawawaki H, Koriyama T, Ri S, et al. Aristaless-related homeobox gene disruption leads to abnormal distribution of GABAergic interneurons in human neocortex: evidence based on a case of X-linked lissencephaly with abnormal genitalia (XLAG). Acta Neuropathol 2008; 116: 453–62.

Parnavelas JG. The origin and migration of cortical neurones: new vistas. Trends Neurosci 2000; 23: 126–31.

Pettersen EF, Goddard TD, Huang CC, Couch GS, Greenblatt DM, Meng EC, et al. UCSF Chimera: a visualization system for exploratory research and analysis. J Comput Chem 2004; 25: 1605–12.

Romaniello R, Arrigoni F, Panzeri E, Poretti A, Micalizzi A, Citterio A, et al. Tubulin-related cerebellar dysplasia: definition of a distinct pattern of cerebellar malformation. Eur Radiol 2017; 27: 5080–92.

Roosing S, Romani M, Isrie M, Rosti RO, Micalizzi A, Musaev D, et al. Mutations in CEP120 cause Joubert syndrome as well as complex ciliopathy phenotypes. J Med Genet 2016; 53: 608–15.

Rubenstein JL, Puelles L. Homeobox gene expression during development of the vertebrate brain. Curr Top Dev Biol 1994; 29: 1–63.

Sarnat HB. Molecular genetic classification of central nervous system malformations. J Child Neurol 2000; 15: 675–87.

Severino M, Tortora D, Pistorio A, Ramenghi LA, Napoli F, Mancardi MM, et al. Expanding the spectrum of congenital anomalies of the diencephalic-mesencephalic junction. Neuroradiology 2016; 58: 33–44.

Simons C, Wolf NI, McNeil N, Caldovic L, Devaney JM, Takanohashi A, et al. A de novo mutation in the β-tubulin gene TUBB4A results in the leukoencephalopathy hypomyelination with atrophy of the basal ganglia and cerebellum. Am J Hum Genet 2013; 92: 767–73.

Singh G, Kaur S, Stock JL, Jenkins NA, Gilbert DJ, Copeland NG, et al. Identification of 10 murine homeobox genes. Proc Natl Acad Sci U S A 1991; 88: 10706–10.

Smart IH. Differential growth of the cell production systems in the lateral wall of the developing mouse telencephalon. J Anat 1985; 141: 219–29.

Smart IH, McSherry GM. Growth patterns in the lateral wall of the mouse telencephalon. II. Histological changes during and subsequent to the period of isocortical neuron production. J Anat 1982; 134: 415–42.

Spieler D, Baumer N, Stebler J, Koprunner M, Reichman-Fried M, Teichmann U, et al. Involvement of Pax6 and Otx2 in the forebrain-specific regulation of the vertebrate homeobox gene ANF/Hesx1. Dev Biol 2004; 269: 567–79.

Szucsik JC, Witte DP, Li H, Pixley SK, Small KM, Potter SS. Altered forebrain and hindbrain development in mice mutant for the Gsh-2 homeobox gene. Dev Biol 1997; 191: 230–42.

Thion MS, Ginhoux F, Garel S. Microglia and early brain development: an intimate journey. Science 2018; 362: 185–9.

Toresson H, Potter SS, Campbell K. Genetic control of dorsal-ventral identity in the telencephalon: opposing roles for Pax6 and Gsh2. Development 2000; 127: 4361–71.

Tucker RP. The roles of microtubule-associated proteins in brain morphogenesis: a review. Brain Res Rev 1990; 15: 101–20.

Valerius MT, Li H, Stock JL, Weinstein M, Kaur S, Singh G, et al. Gsh-1: a novel murine homeobox gene expressed in the central nervous system. Dev Dyn 1995; 203: 337–51.

Wang B, Waclaw RR, Allen ZJ, 2nd, Guillemot F, Campbell K. Ascl1 is a required downstream effector of Gsx gene function in the embryonic mouse telencephalon. Neural Dev 2009; 4: 5.

Webb B, Sali A. Comparative protein structure modeling using MODELLER. Curr Protoc Bioinform 2014; 47: 1–32.

Yun K, Potter S, Rubenstein JL. Gsh2 and Pax6 play complementary roles in dorsoventral patterning of the mammalian telencephalon. Development 2001; 128: 193–205.

Zaki MS, Saleem SN, Dobyns WB, Barkovich AJ, Bartsch H, Dale AM, et al. Diencephalic-mesencephalic junction dysplasia: a novel recessive brain malformation. Brain 2012; 135: 2416–27.

Zhao X, Huang XR, Sun CC. Molecular dynamics analysis of the engrailed homeodomain-DNA recognition. J Struct Biol 2006; 155: 426–37.

Zuccoli G, Yannes MP, Nardone R, Bailey A, Goldstein A. Bilateral symmetrical basal ganglia and thalamic lesions in children: an update. Neuroradiology 2015; 57: 973–89.